Switch on, switch off: stiction in nanoelectromechanical switches

2013 Nanotechnology 24 275501

(http://iopscience.iop.org/0957-4484/24/27/275501)

Nanotechnology **24** (2013) 275501 (11pp) doi:10.1088/0957-4484/24/27/275501

Switch on, switch off: stiction in nanoelectromechanical switches

Till J W Wagner[1] **and Dominic Vella**[2]

[1] Department of Applied Mathematics and Theoretical Physics, University of Cambridge, Wilberforce Road, Cambridge CB3 0WA, UK
[2] OCCAM, Mathematical Institute, University of Oxford, 24-29 St Giles', Oxford OX1 3LB, UK

E-mail: twagner@cantab.net

Received 19 February 2013, in final form 7 May 2013
Published 13 June 2013
Online at stacks.iop.org/Nano/24/275501

Abstract
We present a theoretical investigation of stiction in nanoscale electromechanical contact switches. We develop a mathematical model to describe the deflection of a cantilever beam in response to both electrostatic and van der Waals forces. Particular focus is given to the question of whether adhesive van der Waals forces cause the cantilever to remain in the 'ON' state even when the electrostatic forces are removed. In contrast to previous studies, our theory accounts for deflections with large slopes (i.e. geometrically nonlinear). We solve the resulting equations numerically to study how a cantilever beam adheres to a rigid electrode: transitions between 'free', 'pinned' and 'clamped' states are shown to be discontinuous and to exhibit significant hysteresis. Our findings are compared to previous results from linearized models and the implications for nanoelectromechanical cantilever switch design are discussed.

(Some figures may appear in colour only in the online journal)

1. Introduction

As the size of electronic systems is scaled down further and further, nanoelectromechanical (NEM) devices are increasingly seen as the 'promised land' of truly nanoscale technology. The development of NEM contact switches is often taken to be the natural next step from conventional semiconductor systems and has received much attention in recent research—see the review by Loh and Espinosa [1] for an overview of this area.

The concept of (macroscopic) electromechanical contact switches dates back to the early days of the telephone. It is, perhaps, the simplest example of how electrical and mechanical forces interact: an externally applied voltage induces mechanical bending of an electrode and closes the circuit. Once the voltage is removed, the elasticity of the electrode causes the switch to open again. However, as the size of the system is reduced to micro and nanoscales, a third force (in addition to the electrostatic and elastic forces) becomes significant: the short range van der Waals (vdW) attraction between the electrodes. If this attraction is sufficiently strong then, once driven into contact by electrostatic forces, the switch may become 'stuck' in the ON position and may not reopen—even when the voltage is removed. This phenomenon, known as stiction failure, is one of two main engineering difficulties in modern NEM switch design (the other being 'ablation', in which the tip of the electrode is damaged by repeated contact cycles).

In this paper we present a model of the operation of a NEM switch that incorporates three aspects of the stiction problem that previously have been considered in isolation: (a) the pull-in/pull-out behaviour of contact switches, for combined vdW–Coulomb interactions; (b) the different adhered states possible and the transition between these states; (c) the effect of geometric nonlinearities for systems that feature large deflections. We first review briefly the previous work on each of these aspects.

The ON/OFF cycle of a cantilever switch is characterized by the transition from the freely suspended state to a contact state upon the application of a voltage difference (pull-in) and the transition from a contact state back to the free state upon the removal of that voltage difference (pull-out). The pull-in behaviour of microelectromechanical (MEM) switches was first studied by considering a beam responding to electrostatic forces alone [2, 3]. As the interest in NEM devices increased, these models were superseded by models of a beam subjected

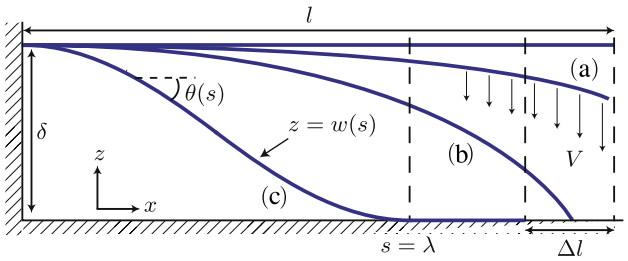

Figure 1. Cantilever beam of length l, suspended at height δ and subject to voltage V. The diagram highlights the three possible states of the beam: (a) freely suspended, (b) pinned at its free end, and (c) adhered to the bottom electrode over a finite distance (detaching at $s = \lambda$). In the process, the free end of the beam is displaced by a horizontal distance Δl. The shape of the beam is characterized by the intrinsic angle $\theta(s)$.

to a combination of vdW and Coulomb forces. This made it possible to obtain an analytical estimate of the pull-in voltage for carbon-nanotube (CNT) based NEM switches [4]. Later, these models also incorporated capillary and non-classical effects such as combined vdW–Casimir interactions [5, 6]. Much of the recent experimental and numerical work has been based on this vdW–Coulomb model [7, 8]. However, the stiction conditions derived from this usually assume that the pull-out voltage is identical to the pull-in voltage [8] and hence preclude the possibility of hysteresis due to adhesion. More recently, hysteretic adhesion was investigated by looking at a beam with a dimple at its free end [9]. This gives rise to adhesion over a finite length (the length of the dimple) as soon as the beam makes contact with the substrate. Such a state is known as a 'clamped' state—(c) in figure 1. In the absence of a dimple, however, stiction can still occur even when the contact length tends to zero. The beam is then 'pinned' to the substrate at the end—(b) in figure 1.

The two different modes of stiction for cantilever beams—'pinned' and 'clamped'—were investigated in the context of stiction failure in MEM switches [10–12]. Stiction conditions for both pinned and clamped states have been presented, together with studies of the transition between them [13, 14]. These conditions give bounds for the design parameters of contact switches to avoid irreversible stiction and can also be used to estimate the strength of adhesion of an adhered beam [13, 15, 16]. Even though both clamped and pinned states are known to occur in NEM switches this earlier work is often ignored in later literature [3, 17]. More recently, adhesion transitions of multiple flexible sheets were investigated using a general approach [18]. This established a hysteresis loop between the different adhered (and non-adhered) states.

A common simplification in previous studies of cantilever switches is that the switch deformation has a small slope so that a linearized beam theory is appropriate. However, examples in the literature suggest that many modern NEM contact switches feature relatively large switch height/beam length aspect ratios [1, 17]. In such cases, the assumption of small slopes is no longer appropriate—a nonlinear approach is called for. To our knowledge, large deflections have not been considered in previous studies of the stiction of contact switches (some studies, such as Ramezani *et al* [19] account for large deflections, but only up to pull-in). However, studies have considered nonlinear effects in systems that are related to the cantilever switch, including the peeling of a thin elastica from an adhesive substrate [20], the folding of an elastica upon itself [21] and the shape of large delamination blisters [22]; these examples are all reminiscent of a cantilever switch in its ON state.

In this paper, we present a nonlinear model of a cantilever switch undergoing large elastic deflections due to a combination of vdW and Coulomb forces. We study how the suspended and adhered states change qualitatively with increasing and decreasing applied voltage and characterize the geometric and material conditions that result in permanent stiction.

2. Theoretical formulation

2.1. Problem setup

We consider a naturally flat beam, of length l, width a, and thickness h, acting as an electrode, suspended above a second, rigid electrode (the substrate). This setup is shown schematically in figure 1. The beam is clamped at a height δ above the substrate at one end and is free at the other end. The system is subjected to an externally applied voltage, so that the beam experiences an electrostatic force that causes it to bend towards the bottom electrode. The voltage is increased until the beam makes contact with the substrate—at a critical pull-in voltage $V_{\text{p–i}}$. The switch is then said to be in its ON state, since it is now able to conduct. If the voltage is increased beyond $V_{\text{p–i}}$ the beam deflects further and becomes increasingly adhered (but still subject to free boundary conditions at its tip, whereas in the macroscopic picture it now evolves with pinned or clamped boundary conditions at the point of contact). It has been shown previously that a quasi-static approach is justified [19], which allows us to ignore dynamic effects in what follows.

We assume that the material properties of the beam, namely its Young's modulus, E, and Poisson ratio, ν, are given, along with the strength of adhesion between beam and substrate, $\Delta\gamma$, (defined as an adhesive energy per unit area). The system is then characterized by a typical length, known as the *elastocapillary length* [23, 24] defined as $\ell_{\text{ec}} = \sqrt{\mathcal{B}/\Delta\gamma a}$, where $\mathcal{B} = Eah^3/12(1-\nu^2)$ is the bending stiffness for a sheet or wide beam [25]. Qualitatively, our model is also valid for narrow beams, where the bending stiffness is replaced by $\mathcal{B} = Eah^3/12$ [26]. The elastocapillary length is a measure of the relative strengths of the bending stiffness of the sheet and the sheet–substrate adhesion. For given E and ν, ℓ_{ec} may be varied by changing the thickness of the beam (which changes the bending stiffness $\mathcal{B}$), but keeping $\Delta\gamma$ constant. The cantilever system features three geometric lengthscales that can be varied: the thickness of the beam, h, its length l, and the clamping height, δ.

The deflection of the cantilever is determined by modelling the cantilever as an elastic beam. While we account for geometric nonlinearities, such a beam model is only

valid when $h \ll l$ [27]. With this restriction, there are only three possible separations of scale: $h \ll \delta \ll l$, $h \ll \delta \sim l$ and $h \sim \delta \ll l$. The first of these limits is that usually considered in theoretical studies of NEM/MEM contact switches. However, the latter two regimes are becoming increasingly relevant in many nanoscale applications [1, 17]. Considering a geometrically nonlinear model allows us to describe systems where $\delta \sim l$. To account for the case where $h \sim \delta$, it is also important to include the effect of finite beam thickness in the description of the vdW forces.

Our model considers both van der Waals and Coulomb forces. As discussed above, this combination has previously been considered in cantilever switch problems [1, 4, 9]. However, the focus of these studies has been almost exclusively on estimating the pull-in voltage of a system, with little attention paid to the stiction process for voltages beyond pull-in. However, the volatility of stiction (whether stiction remains once the voltage is removed) is determined by the competition of bending moments in the deformed beam (which tend to restore the system to its original undeformed state) and the attractive van der Waals forces, which give rise to the adhesion $\Delta\gamma$ (forcing the beam into an adhered state). It is therefore important to consider the effect of adhesion beyond pull-in.

The Casimir force is neglected in our model. This is motivated by the fact that the Casimir force dominates vdW forces only for beam–substrate separations $w > 50$ nm [28]; for $w < 50$ nm vdW forces dominate. However, by far the most important contribution from intermolecular forces to the state of the beam is found when the sheets are in contact or very close to contact, i.e. $w \ll 50$ nm. Casimir forces may thus be neglected in comparison to vdW forces when considering pull-out transitions. For pull-in transitions on the other hand, electrostatic forces are the most important attractive force, since Casimir forces decay more quickly (like $1/w^4$) than electrostatic forces ($1/w^2$) and, as we shall see shortly, pull-in occurs with macroscopic cantilever–substrate separations.

2.2. Variational formulation

To determine the equations governing the shape of the deflected cantilever beam, we use a variational formulation of the problem. The bending energy per unit length of the beam is written as $U_B = \frac{1}{2}\mathcal{B}\theta_s^2$, where $\theta(s)$ is the angle (measured relative to the horizontal) of the tangent to the curve and $()_s = \mathrm{d}/\mathrm{d}s$. We ignore stretching effects (considered, for example in Yin and Ya-Pu [29]), which is consistent with our later neglecting friction (the validity of this assumption is discussed below) and the requirement that $h \ll l$. The van der Waals interaction energy between a molecule in the cantilever and a molecule in the substrate is then given by [30]

$$U_{\mathrm{m-m}} = -C\left(\frac{1}{r^6} - \frac{D}{r^{12}}\right), \tag{1}$$

with r the distance between the two molecules and C and D material dependent parameters. C is sometimes referred to as the 'London Constant' and has units J m^{-6}, whereas D can be related to the van der Waals radius, which describes the equilibrium contact distance between two objects (see below).

For the case of small inclination angles of the beam to the horizontal, $\theta(s) \ll 1$, (1) yields the following van der Waals energy density for a sheet of thickness h, whose mid-plane is at a height $w(s)$ above a flat substrate [31]:

$$\mathcal{E}_{\mathrm{vdW}}(s) = -\frac{A_H}{12\pi}\left[\left(\frac{1}{(w(s)-h/2)^2} - \frac{1}{(w(s)+h/2)^2}\right) - \frac{D}{30}\left(\frac{1}{(w(s)-h/2)^8} - \frac{1}{(w(s)+h/2)^8}\right)\right] \tag{2}$$

where $A_H \equiv \pi^2 C\rho\rho_s$ is known as the Hamaker constant, and ρ and ρ_s are the densities of sheet and substrate, respectively. We define the van der Waals radius as

$$w^* = w_0 - h/2, \tag{3}$$

where w_0 is the equilibrium contact distance between the mid-plane of the sheet and the substrate surface. w^* is thus the distance between the bottom of the sheet and the top of the substrate, when in contact. Typical values for w^* are ∼2–3 Å, which is much smaller than any of the sheet thicknesses considered. This justifies the assumption that $w^* \ll h$. Making use of (2), it emerges from considerations of equilibrium at $w = w_0$ that $D \simeq (15/2)w^{*6}$.

The effects of large deflections (where $\theta \sim 1$) are included by integrating the energy from $z = w - h/2\cos\theta$ to $z = w + h/2\cos\theta$, for a beam segment at an angle θ to the horizontal. The van der Waals energy density may then be written:

$$\mathcal{E}_{\mathrm{vdW}} = -\frac{A_H}{12\pi}\left[\left(\frac{1}{(w-h/2\cos\theta)^2} - \frac{1}{(w+h/2\cos\theta)^2}\right) - \frac{D}{30}\left(\frac{1}{(w-h/2\cos\theta)^8} - \frac{1}{(w+h/2\cos\theta)^8}\right)\right]. \tag{4}$$

It is common to replace the Hamaker constant A_H with the strength of adhesion, $\Delta\gamma$, defined as the energy required to separate surfaces from the contact distance w_0 to infinity [30]. In the limit $w^* \ll h$, we find

$$\Delta\gamma = \mathcal{E}_{\mathrm{vdW}}(\infty) - \mathcal{E}_{\mathrm{vdW}}(w_0) \simeq \frac{A_H}{16\pi}\frac{1}{w^{*2}}. \tag{5}$$

Writing $w_- \equiv w - h/2\cos\theta$ and $w_+ \equiv w + h/2\cos\theta$, and making use of (5), we rewrite (4) to give the vdW energy per unit length

$$U_{\mathrm{vdW}} = -\frac{4}{3}\Delta\gamma a\left\{\left(\frac{w^*}{w_-}\right)^2 - \left(\frac{w^*}{w_+}\right)^2 - \frac{1}{4}\left[\left(\frac{w^*}{w_-}\right)^8 - \left(\frac{w^*}{w_+}\right)^8\right]\right\}. \tag{6}$$

The Coulomb energy due to an externally applied voltage scales as $U_E \sim w(s)^{-1}$ [30]. This means that the electrostatic potential will be the driver of deflection wherever $w(s) \gg h$ but will be small compared to the vdW term when $w(s) \leq h$, i.e. when the beam is adhered. The fact that the U_E contribution is only significant when $w(s) \gg h$ suggests that

we may neglect the finite thickness of the beam in the electrostatic term. The electrostatic energy (per unit length), defined as the work required to bring the beam from its original separation, where $z(s) = \delta$, to $z(s) = w(s)$, may be written

$$U_{\mathrm{E}}(s) = -\frac{1}{2}\epsilon_0 V^2 a\left(\frac{1}{w(s)} - \frac{1}{\delta}\right), \tag{7}$$

where ϵ_0 is the permittivity of free space. For simplicity, we ignore in this study the effects of fringing fields and do not consider dielectric layers which are commonly used in experimental setups [2, 29, 32, 33]. However, our model could be modified to include these effects by adjusting the prefactor/adding a constant term in (7) accordingly.

To obtain the total free energy, the energies U_{B}, U_{vdW} and U_{E} are integrated over the total length of the beam. The equation of state of the system is then found by minimizing

$$U = \int_0^l [U_{\mathrm{B}}(s) + U_{\mathrm{vdW}}(s) + U_{\mathrm{E}}(s) + F(s)(w_s - \sin\theta) + T(s)(x_s - \cos\theta)]\,\mathrm{d}s, \tag{8}$$

where $F(s)$ and $T(s)$ are Lagrange multipliers associated with the geometric relations

$$w(s) = \int_0^s \sin\theta(s')\,\mathrm{d}s', \qquad x(s) = \int_0^s \cos\theta(s')\,\mathrm{d}s'. \tag{9}$$

The Lagrange multipliers $F(s)$ and $T(s)$ correspond physically to the vertical and horizontal components of the internal stress acting within the beam, respectively [26].

In what follows, it will be helpful to rescale all lengths by l, writing

$$d = \delta/l, \quad S = s/l, \quad H = h/l, \quad W = w/l, \quad \text{etc.} \tag{10}$$

We then obtain

$$\mathcal{U} = \int_0^1 \left\{\frac{1}{2}\theta_S^2 - \frac{\alpha}{2}\left[\left(\frac{1}{W_-^2} - \frac{1}{W_+^2}\right) - \frac{\beta}{4}\left(\frac{1}{W_-^8} - \frac{1}{W_+^8}\right)\right] - \psi\left(\frac{1}{W} - \frac{1}{d}\right) + \eta(W_S - \sin\theta) + \tau(X_S - \cos\theta)\right\}\mathrm{d}S,$$

where, $\mathcal{U} = Ul/\mathcal{B}$ is the dimensionless Lagrangian and

$$\alpha \equiv A_{\mathrm{H}}a/6\pi\mathcal{B}, \quad \beta \equiv 2D/15l^6, \quad \psi \equiv \epsilon_0 V^2 a l/2\mathcal{B}, \quad \eta \equiv Fl^2/\mathcal{B}, \quad \tau \equiv Tl^2/\mathcal{B}. \tag{11}$$

We define the dimensionless strength of adhesion $\Gamma \equiv l^2\Delta\gamma a/\mathcal{B}$, such that $\alpha \simeq (8/3)W^{*2}\Gamma$ in the limit $W^* \ll H$, and $\beta \simeq W^{*6}$. We simplify our notation by writing the sum of vdW and Coulomb energies as $\mathcal{G}(W,\theta) = \mathcal{U}_{\mathrm{vdW}} + \mathcal{U}_{\mathrm{E}}$.

Using the Calculus of Variations, we find that the functional $\mathcal{U}$ is extremized by functions θ, X, W, η, and τ satisfying:

$$\begin{aligned} &\theta_{SS} + \eta(S)\cos\theta + \tau(S)\sin\theta + \mathcal{G}_\theta = 0, \\ &\eta_S - \mathcal{G}_W = 0, \qquad \tau_S = 0, \\ &W_S = \sin\theta, \qquad X_S = \cos\theta. \end{aligned} \tag{12}$$

From the third equation in (12) it is clear that τ is constant. However, since no horizontal force is applied to the end of the beam we find that the internal stress in the X-direction at $S = 1$ is zero and therefore $\tau = 0$ everywhere.

Finally, our model neglects friction between the cantilever and the substrate. We neglect friction to simplify the treatment of contact regions. However, we note that experimental measurements of the friction coefficient of graphene layers yielded very low values (around 0.03, [34]), so that frictional forces are always negligible in comparison to normal forces. Incorporating friction would also require a changing stress within the contacting part of the cantilever [35] which is inconsistent with the third equation in (12).

With $\tau = 0$, equation (12) reduces to a system of one second order ODE and three first order ODEs. Therefore, five boundary conditions are required to solve the system: these are given by

$$\begin{aligned} X(0) = 0, \quad W(0) = d, \quad \theta(0) = 0, \\ \theta_S(1) = 0, \quad \eta(1) = 0. \end{aligned} \tag{13}$$

The first three of these fix the beam to be clamped at a height d, at $S = 0$. The third and fourth impose free end boundary conditions at $S = 1$. Note that, since adhesion is modelled by an attractive potential, these free end conditions apply to all states of the switch—whether they are adhered or not. In contrast, theoretical treatments without explicit vdW forces instead impose adhesion conditions at the stuck end of the beam, which modifies the boundary conditions (13)—such models are discussed below.

To compute the horizontal deflection of the free end, ΔL, for given input parameters d, H, ψ, we use the geometrical relationship

$$\Delta L = \int_0^1 1 - \cos\theta\,\mathrm{d}S, \tag{14}$$

once we have solved for the beam shape $\theta(S)$.

3. Numerical procedure and results

The system (12) subject to the boundary conditions (13) can readily be solved using the MATLAB boundary value problem solver `bvp4c`. As the applied voltage is increased or decreased, the evolution of the cantilever shape can be traced using a straight-forward continuation scheme. Resulting deflection profiles are shown in figure 2.

We observe two distinct contact states: an arc-shaped, or *pinned*, state (profile (c) in figure 2), and an s-shaped, or *clamped*, state (profile (d)). We analyse the evolution of the switch as the applied voltage, ψ is varied, paying particular attention to the appearance of these adhered states. It is convenient to present this evolution in terms of the horizontal displacement of the free end, ΔL, since the transition between free, pinned and clamped states is marked by observable jumps in ΔL (see figures 4, 6 and 7). Furthermore, in each of the observed states, ΔL evolves in qualitatively different ways with ψ: for the suspended beam, ΔL grows rapidly up to the pull-in voltage $\psi_{\mathrm{p-i}}$; for the pinned state, ΔL decreases slightly with increasing ψ; finally, the clamped state features

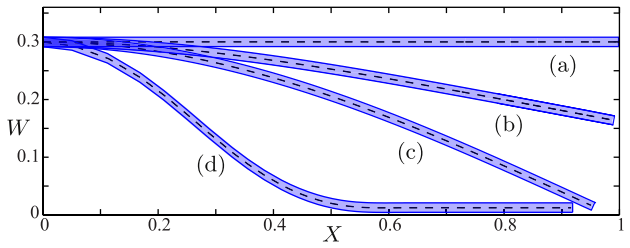

Figure 2. Switch profiles for $d = 0.3$, $H = 0.01$ and different applied voltages, ψ: (a) $\psi = 0$, no deflection; (b) $\psi \approx \psi_{\text{p–i}}$, suspended state just before snap-through; (c) pinned configuration, $\psi_{\text{pin}}^{(\text{min})} < \psi < \psi_{\text{pin}}^{(\text{max})}$; (d) clamped configuration, $\psi > \psi_{\text{clamp}}^{(\text{min})}$ (see text).

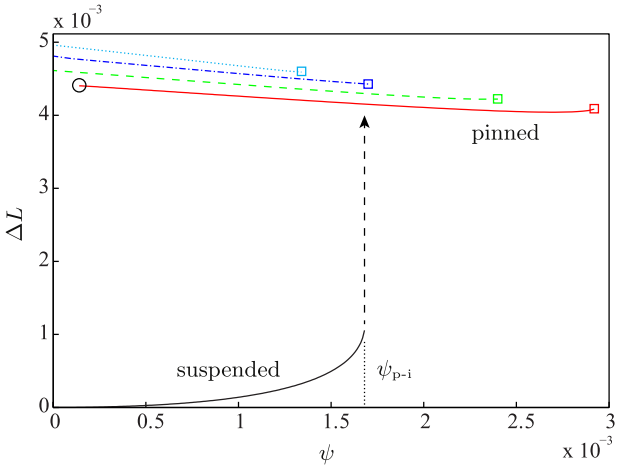

Figure 3. $\Delta L(\psi)$ for four different beam thicknesses H, showing suspended and pinned states (clamped states are omitted for clarity). Curves are shown for beams clamped at height $d = 0.1$ with thicknesses $H = 0.005$ (cyan dotted), $H = 0.007$ (blue dash-dotted), $H = 0.012$ (green dashed) and $H = 0.016$ (red solid). The squares mark the respective values for $\psi_{\text{pin}}^{(\text{max})}(H)$ (at which point the beam becomes clamped). The $\Delta L(\psi)$ dependence for freely suspended states is approximately independent of H, yielding indistinguishable curves for different heights (black curve at base), with maximum value $\psi_{\text{p–i}}$. The dashed arrow marks the transition from suspended-to-pinned states. The black circle marks volatile pinned stiction for the thickest sheet.

again a monotonic increase, where $\Delta L \to d$ as $\psi \to \infty$. (The decrease in ΔL for the pinned state is due to the increased attraction over the length of the beam, leading to the tip being pushed outwards.)

In general, the evolution of the switch with ψ runs along a hysteresis loop (illustrated in figures 4, 6 and 7): starting from a freely suspended beam, the system snaps to a pinned or clamped adhered state at $\psi_{\text{p–i}}$. Once pinned, the beam will transition to a clamped configuration at a critical voltage $\psi_{\text{pin}}^{(\text{max})}$ and remain in the clamped state as ψ is increased further. As ψ is reduced the beam will either remain in the clamped state or transition back to the pinned state (at $\psi_{\text{clamp}}^{(\text{min})}$) and remain there as $\psi \to 0$, exhibiting non-volatile stiction in both cases. Otherwise, it will return to the freely suspended state for $0 < \psi < \psi_{\text{pin}}^{(\text{min})}$ (volatile stiction). In the remainder of this section we will discuss the properties of this hysteresis loop in some detail.

We first consider the pull-in process as ψ is increased up to $\psi_{\text{p–i}}$ by looking at how the transition from suspended to adhered states is dependent on the switch parameters d and H. We then examine volatile and non-volatile stiction behaviour as ψ is decreased to zero.

We solve equations (12) and (13) for given values of the dimensionless parameters d, H, W^* and Γ. To guide the values of these parameters used in our calculations, we first consider a set of typical dimensional values for carbon-based NEM switch design. The strength of adhesion for graphene on different substrates has been reported to lie in the range $\Delta\gamma \simeq 0.04$–0.3 J m^{-2} [36–38]. We take $\Delta\gamma = 0.065$ J m^{-2}, which corresponds to typical carbon–carbon adhesion [30], one of the scenarios discussed by Loh and Espinosa [17]. The bending stiffness (per unit area) of few layered graphene can be approximated by $\mathcal{B}/a = bn^3$, where $b \simeq 18$ eV is the scaled bending stiffness and n is the number of molecular layers in the beam [39]. For example, a 30 layered graphene beam has thickness $h = 30h_1 \simeq 10$ nm (where $h_1 \simeq 0.33$ nm is the thickness of a graphene monolayer) and hence a bending stiffness $\mathcal{B}/a \simeq 7.8 \times 10^{-14}$ J. Typical beam lengths are 0.5–1.5 μm [17]. Taking $l = 1$ μm we find $H = 0.01$ and a dimensionless strength of adhesion $\Gamma \simeq 0.08$. The dimensionless vdW radius is $W^* = 3.3 \times 10^{-4}$. In recent experiments, the switch height/beam length aspect ratio typically takes values $d \simeq 0.01$–0.65 [32, 39]. In what follows, we will take the parameters $\Delta\gamma$, b and W^* fixed to the values above. The only quantities that are varied are d and H (and finally l, to obtain figure 8).

3.1. Pull-in transitions

As ψ is increased, the initially straight beam gradually bends towards the bottom electrode, until it jumps to an adhered state at $\psi = \psi_{\text{p–i}}$. Whether this jump is to a pinned or to a clamped adhered state depends on both the switch height d and the beam thickness H.

In the limit $H \ll d$, the pinned state is extremely unstable, which is to say that numerical solutions are not found for thicknesses lower than a critical value, for given d. The reason for this is the following. The larger d, the greater the slope at the point of contact, $\theta(1)$. Consequently, the short range vdW forces act only on the very tip of the beam. As H becomes small, the contact region tends to zero, making a suspended-to-pinned transition less and less favourable (see figure 3).

We find that the stability of pinned states is also restricted in the limit $d \sim H \ll 1$. In this limit, the slope of the beam is small and the vdW forces act on a significant length of the beam. This causes the beam to 'zip up' and so the clamped configuration is again favoured over the pinned one (see figure 4). The dependence of these transitions on d and H can be quantified by looking at the critical voltages $\psi_{\text{p–i}}(d, H)$ and $\psi_{\text{pin}}^{(\text{max})}(d, H)$.

Our numerical results suggest that the pull-in voltage is approximately independent of H and scales as $\psi_{\text{p–i}} \sim d^3$. Computing a best fit power law gives $\psi_{\text{p–i}} \approx 1.702d^3$

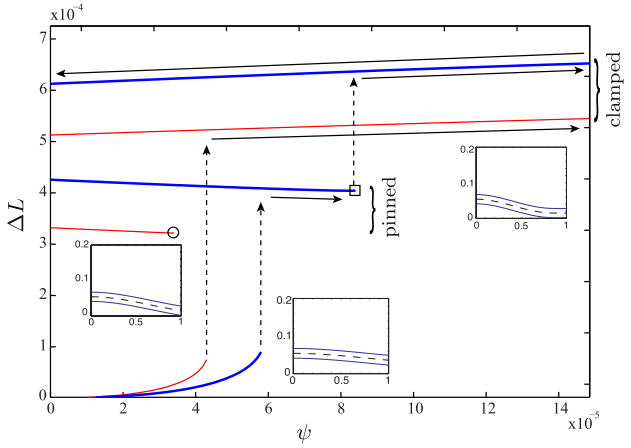

Figure 4. The dependence of ΔL on ψ, for a beam of thickness $H = 0.012$ and suspended at heights $d = 0.030$ (red thin) and $d = 0.033$ (blue thick). The black circle and square correspond to the maximally adhered pinned states which are marked in figure 5. Dashed arrows show transitions between states, solid arrows illustrate the continuous evolution of each different state with varying voltage. Insets: profiles corresponding to the different (suspended, pinned, clamped) states.

(represented by the solid line in figure 5(a)). This scaling is in agreement with previous analytical estimates [2, 4] of $\psi_{\text{p–i}}(d)$, which calculated the (dimensional) pull-in voltage for a cantilever switch to be

$$V_{\text{p–i}} = \sqrt{\frac{32}{27}\left(\frac{2\mathcal{B}}{\epsilon_0 a l}\right)\left(\frac{\delta}{l}\right)^3}. \qquad (15)$$

In dimensionless terms this becomes $\psi_{\text{p–i}} = (\epsilon_0 a l/2\mathcal{B})V_{\text{p–i}}^2 \approx 1.185 d^3$. While the previously determined prefactor is lower than that found in our numerics, we note that in the derivation of (15) the pull-in height is taken to be $w(l) = (2/3)\delta$. This value is based on the assumption that the electrostatic force, f_{E}, acts uniformly over the length of the beam, with its strength calculated based solely on the separation at the end of the beam. In reality, this overestimates f_{E} (and hence underestimates the pull-in voltage), since the free end is the point closest to the substrate; in fact f_{E} is significantly smaller towards the clamped end (at $s = 0$). Our model, on the other hand, computes pull-in explicitly, accounting for non-uniform f_{E}; as a rule of thumb, we find deflections consistently closer to $w(l) \simeq (1/2)\delta$.

Figures 3 and 4 show the evolution of $\Delta L(\psi)$. We find that transitions occur at $\psi = \psi_{\text{p–i}}$ and that the transition is from

$$\text{suspended} \rightarrow \text{pinned}, \qquad \text{for } \psi_{\text{p–i}}(d) < \psi_{\text{pin}}^{(\max)}(d, H),$$

but from

$$\text{suspended} \rightarrow \text{clamped}, \qquad \text{for } \psi_{\text{p–i}}(d) > \psi_{\text{pin}}^{(\max)}(d, H).$$

The functions $\psi_{\text{p–i}}(d)$ and $\psi_{\text{pin}}^{(\max)}(d)$ are shown in figure 5(a), for $H = 0.012$. Critical heights demarcating the modes of transition, are given by the solutions to

$$\psi_{\text{pin}}^{(\max)}(d, H) = \psi_{\text{p–i}}(d). \qquad (16)$$

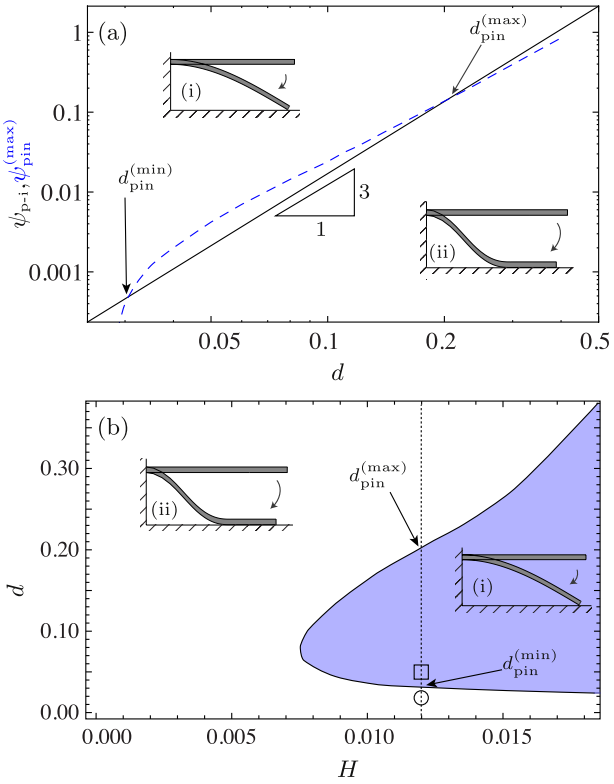

Figure 5. (a) Log–log plots of transition voltages $\psi_{\text{p–i}}(d)$ (solid black) and $\psi_{\text{pin}}^{(\max)}(d)$ (blue dashed), for $H = 0.012$. When $\psi_{\text{pin}}^{(\max)} > \psi_{\text{p–i}}$, transitions from suspended-to-pinned states are observed—inset (i). When $\psi_{\text{pin}}^{(\max)} < \psi_{\text{p–i}}$, the system jumps straight from suspended-to-clamped states—inset (ii). Critical switch heights $d_{\text{pin}}^{(\min)}$ and $d_{\text{pin}}^{(\max)}$ are shown, demarcating the boundary between the two transitions. The scaling $\psi_{\text{p–i}} \sim d^3$ is illustrated. (b) Regime diagram of pull-in transitions in (d, H) space. The blue area represents (d, H) values where the suspended $\rightarrow$ pinned transition is possible; the dotted line represents $H = 0.012$, with $d_{\text{pin}}^{(\max)}$ and $d_{\text{pin}}^{(\min)}$ as above. Circle and square correspond to the configurations shown in figure 4.

Interestingly, (16) has no solutions for thicknesses less than a critical value $H_{\text{pin}} \simeq 0.0072$, which means that for $H < H_{\text{pin}}$ the beam snaps from the freely suspended straight to the clamped state for all values of d. For $H = H_{\text{pin}}$, there is only one solution to (16), $d_{\text{pin}} \simeq 0.083$. For $H > H_{\text{pin}}$, there are two solutions, which we label $d_{\text{pin}}^{(\min)}$ and $d_{\text{pin}}^{(\max)}$. These results may be summarized in a regime diagram illustrating the parameter ranges for which each of the two contact (or adhesion) transitions occur—see figure 5(b).

Figure 5 shows that the beam can only transition from suspended-to-pinned when $H > H_{\text{pin}}$ and $d_{\text{pin}}^{(\min)} < d < d_{\text{pin}}^{(\max)}$. Taking $H = 0.012$, we find $d_{\text{pin}}^{(\min)} = 0.031$, $d_{\text{pin}}^{(\max)} = 0.208$ and the two different scenarios are illustrated in figure 4: suspended $\rightarrow$ clamped for $d = 0.03$ (red thin) and suspended $\rightarrow$ pinned for $d = 0.033$ (blue thick).

3.2. Pull-out transitions: volatile and non-volatile stiction

Section 3.1 was concerned with the process of pull-in as the voltage increases. In this section we examine the conditions

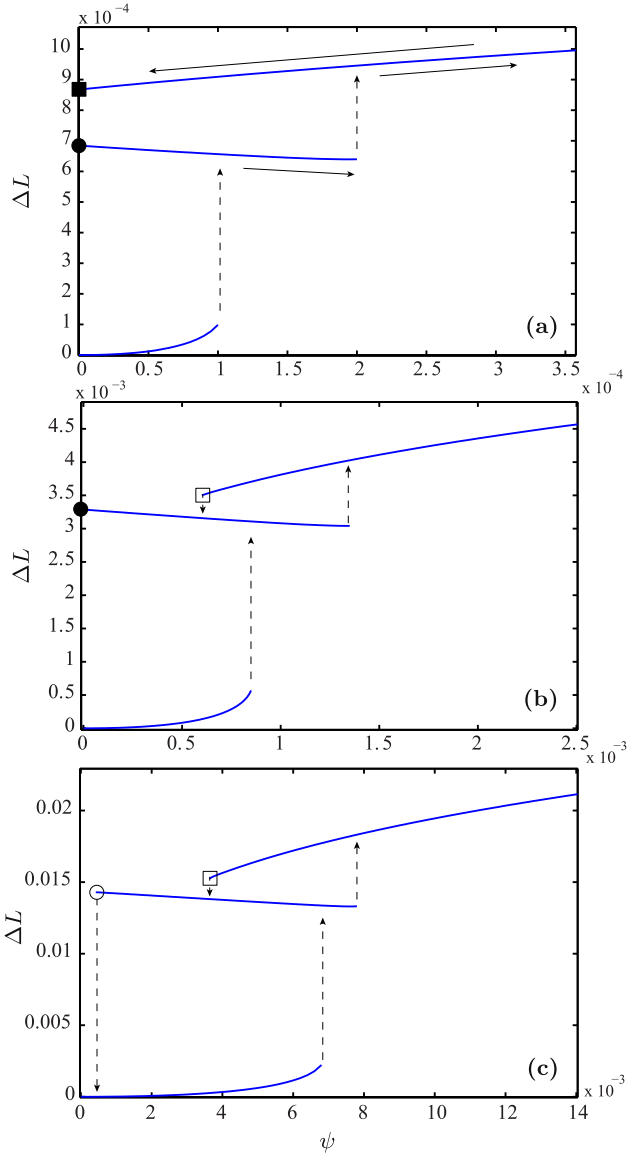

Figure 6. The dependence of ΔL on ψ, for beam thickness $H = 0.012$: (a) $d = 0.04$, (b) $d = 0.08$ and (c) $d = 0.16$. Different curves in each subfigure correspond to suspended, pinned and clamped states, as illustrated in figure 4. Transitions between states are marked as dashed arrows in (a), solid arrows highlight the hysteresis loop for increasing and decreasing voltages. Solid squares and circles mark states with non-volatile clamped and pinned stiction, respectively. Empty squares and circles mark clamped and pinned states exhibiting volatile stiction.

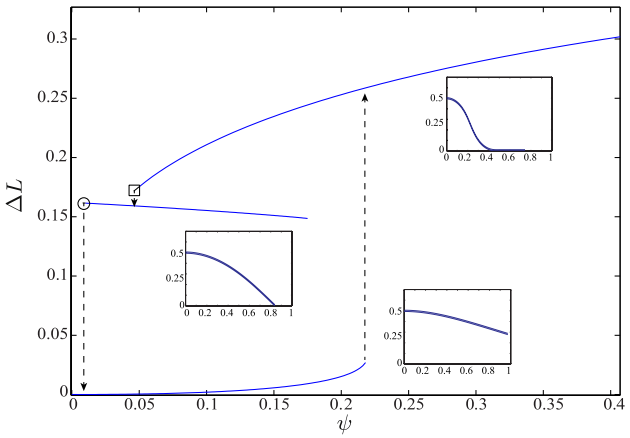

Figure 7. $\Delta L(\psi)$ for the large deflection case, $d = 0.5$ ($H = 0.012$). Empty squares and circles again mark volatile clamped and pinned stiction, respectively. Insets show example profiles of the beam in each of the three possible states.

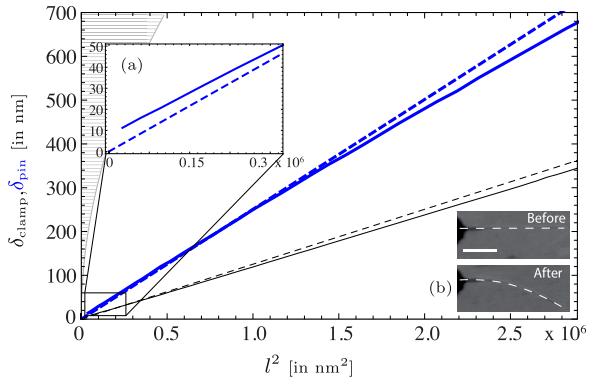

Figure 8. Stiction boundaries for pinned (blue thick) and clamped (black thin) states. The dashed curves give the linear asymptotic results for clamping (19) and pinning (21). The lined region represents the geometrically inaccessible region $\delta > l$, in which no voltage is strong enough to induce contact and hence the switch does not work. Inset (a): detail of the limit $H \sim d$. Inset (b): pinned non-volatile stiction shown on scanning electron micrographs, scale bar is 500 nm. Reproduced with permission from [17]. Copyright 2010 Wiley. (Dashed lines added by authors to highlight the beam shape.)

under which contact remains when the applied voltage is removed; i.e. the conditions under which stiction failure occurs.

To study the limits of non-volatile stiction, we assume that the system is in its clamped state with a given maximum voltage $\psi_{\max}$. As the voltage is decreased the switch will remain in this state until it reaches $\psi^{(\min)}_{\text{clamp}}$. It will then transition to one of the other states as the voltage is decreased further (figure 6). Our numerical results suggest that $\psi^{(\min)}_{\text{clamp}} < \psi^{(\max)}_{\text{pin}}$ for all values of d and H, i.e. there is hysteresis between the two states. Since we also consistently find that $\psi^{(\min)}_{\text{pin}} < \psi^{(\min)}_{\text{clamp}}$, we observe that the clamped state will always transition to the pinned, rather than the suspended state. As the voltage is reduced to zero, we find that clamped stiction may remain, i.e. that $\psi^{(\min)}_{\text{clamp}}(d, H) < 0$ for some values of d and H. This is referred to as non-volatile clamped stiction, since stiction remains even when the voltage that caused it is removed. It is natural to ask, for a given thickness H, what is the minimum device height d needed to avoid non-volatile clamped stiction? This height d_{clamp} is found by solving

$$\psi^{(\min)}_{\text{clamp}}(d, H) = 0.$$

For $d < d_{\text{clamp}}$, the switch will remain in the clamped state when ψ is reduced to zero, whereas, for $d > d_{\text{clamp}}$, the state will transition to pinned when $\psi < \psi^{(\min)}_{\text{clamp}}$.

As ψ is further decreased below $\psi_{\text{clamp}}^{(\text{min})}$ the system remains in its pinned state until $\psi = \psi_{\text{pin}}^{(\text{min})}$. Again, if $\psi_{\text{pin}}^{(\text{min})} < 0$ we expect non-volatile stiction and the solution of $\psi_{\text{pin}}^{(\text{min})} = 0$ gives rise to a minimum device height to avoid non-volatile pinning, d_{pin}. For $0 < \psi < \psi_{\text{pin}}^{(\text{min})}$, the switch will be released and return to its freely suspended state. Volatile stiction is thus observed whenever $\psi_{\text{pin}}^{(\text{min})} > 0$. This hysteresis loop is shown in figures 6 and 7. Figure 6 illustrates the different stiction scenarios: clamped for $d < d_{\text{clamp}}$ (a), pinned for $d_{\text{clamp}} < d < d_{\text{pin}}$ (b) and free when $d > d_{\text{pin}}$ (c).

Figure 7 illustrates the behaviour of the switch in the large deflection regime, i.e. $d = \mathcal{O}(1)$, for the specific case $d = 0.5$ and $H = 0.012$. The evolution of $\Delta L(\psi)$ is found to be qualitatively similar to that already discussed for the limit $d \ll 1$. As argued above (and illustrated in figure 5), we observe a suspended-to-clamped transition in this case, since $d > d_{\text{pin}}^{(\text{max})}$.

From an experimental point of view d_{pin} is likely to be the most important parameter, since systems with $d > d_{\text{pin}}$ will exhibit volatile stiction, while those with $d < d_{\text{pin}}$ will exhibit some form of non-volatile stiction. By fixing ℓ_{ec} (i.e. $\mathcal{B}$ and $\Delta\gamma$) and varying the switch length l, we can compute dimensional values for boundary heights $\delta_{\text{clamp}}(l)$ and $\delta_{\text{pin}}(l)$ (figure 8). These conditions specify the minimum height of a switch required to avoid stiction failure (for given material parameters and beam length).

4. Linear stiction boundaries

We have seen that the question of most practical interest is whether a system undergoes volatile or non-volatile stiction, i.e. when does the beam's state at zero external voltage remain adhered? To gain physical and analytical insight, we consider the small deformation limit (where $\mathrm{d}w/\mathrm{d}x \ll 1$). In this limit, the shape of the cantilever with no applied voltage satisfies the beam equation

$$\mathcal{B}w'''' = 0. \tag{17}$$

In the case of clamped adhesion, the boundary conditions are given by $w(\lambda) = w'(\lambda) = 0$, where λ is the x-coordinate of the point at which contact first occurs (see figure 1). At the origin, the clamped beam boundary conditions remain the same as for the nonlinear theory, namely $w(0) = \delta$, $w'(0) = 0$. We therefore have a fifth order system, since λ is not known *a priori*. An additional condition is then required, which can be shown to be [12, 25, 40]

$$w''(\lambda) = \sqrt{2}/\ell_{\text{ec}}. \tag{18}$$

This geometric relation arises from performing a variation in the position of the point of contact, λ, when minimizing the total free energy of the system.

From this it is a simple matter to derive an expression of the critical switch dimensions for given material characteristics. We find [12, 13]

$$\delta_{\text{clamp}} = (\sqrt{2}/6)l^2/\ell_{\text{ec}}, \tag{19}$$

i.e. for given ℓ_{ec} and l, the maximum switch height that the clamped state supports (where $\lambda = l$) is $\delta = \delta_{\text{clamp}}$. Put another way, to avoid non-volatile stiction one should ensure $\delta > \delta_{\text{clamp}}$.

For pinned states, the boundary conditions are given by $w(l) = w''(l) = 0$. Equation (17) is thus fully determined by the four given boundary conditions (since, in this case, $\lambda = l$). In order to find the critical switch height, we balance the van der Waals and restoring bending forces at the pinned end of the beam, which leads to the 'pinning condition'

$$|w'(l)w'''(l)| = 1/\ell_{\text{ec}}^2, \tag{20}$$

a derivation of which is presented in the appendix. Imposing (20) on the solution of the pinned beam, we find

$$\delta_{\text{pin}} = (\sqrt{2}/3)l^2/\ell_{\text{ec}}. \tag{21}$$

Comparing (19) and (21) we have $\delta_{\text{pin}} = 2\delta_{\text{clamp}}$. This means that the switch has to be twice as high as the clamped stiction condition predicts to avoid pinned stiction.

In this linearized model, the pinned and clamped regimes have a qualitative difference: for given ℓ_{ec} and l, the system can feature clamped states for all heights that satisfy $0 < \delta < \delta_{\text{clamp}}$; however, only one height, namely δ_{pin}, satisfies the conditions for a pinned state. In reality (and in the numerical model presented above), states where $\delta_{\text{clamp}} < \delta < \delta_{\text{pin}}$ adopt an approximately pinned configuration, which features small deformations of the beam near its free end. This is due to the attractive forces being stronger than the restoring force of the ideal pinned state. The finite range of possible close-to-pinned states is illustrated by the slight decrease in ΔL with increasing ψ as discussed in section 3.2.

Note that (21) was derived previously by Mastrangelo and Hsu [10], who arrived at the result by considering shear deformation near the tip when the beam is clamped, letting $\lambda \to l$. However, we believe that the pinning condition (20) and its derivation in the appendix are novel.

4.1. Comparison to nonlinear model

In the regime $h \ll \delta \ll l$, the asymptotic results give numbers that are in good agreement with the numerical results of the nonlinear model, as described in the previous sections. In particular, results for the limits at which the different modes of non-volatile stiction are observed are illustrated in figure 8. It is interesting to observe that good agreement is obtained for relatively large aspect ratios $d = \delta/l$: the upper limit of figure 8 corresponds to $d = 0.3$. This suggests that the boundary conditions (19) and (21) may be applied with reasonable confidence to experimental settings where d is not necessarily small. However, beyond $d \approx 0.3$ the differences between the results of the linear and nonlinear models become increasingly significant.

The lined region in figure 8 represents the geometric constraint $\delta > l$, where contact between beam and substrate is geometrically impossible without stretching. It is important to avoid this region since the switch will not be able to contact and hence will not work.

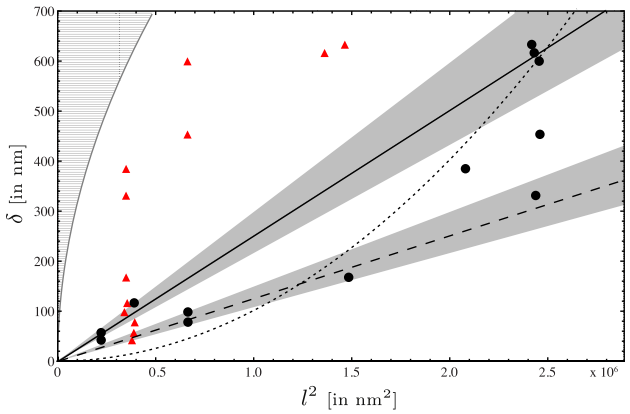

Figure 9. Stiction boundaries δ_{clamp} (dashed) and δ_{pin} (solid), plotted as functions of l^2, giving straight lines, as suggested by (19) and (21). The shaded regions around the boundaries account for the uncertainty in $\Delta\gamma$ and range from $\Delta\gamma = 0.1$ (top limit) to 0.01 J m^{-2} (bottom limit). Red triangles represent experimental data points from systems that exhibit volatile stiction, while black circles represent systems with non-volatile stiction. The dotted line corresponds to the scaling law $\delta \sim l^4$, presented in [17].

Figure 8, inset (a) highlights the divergence of asymptotic and numerical results when $h \sim \delta$. This is due to the effects of the finite beam thickness on the vdW forces.

A scanning electron micrograph is shown in figure 8 (inset (b), reproduced from Loh and Espinosa [17]), which highlights, firstly, that deflections in modern applications are not necessarily small and, secondly, that pinning is possibly the most relevant state when assessing stiction failure of a NEM switch.

4.2. Comparison to experimental data

Finally, we compare the stiction boundaries presented here to experimental data, published in [17] and reproduced in the review by Loh and Espinosa [1]. This experimental data was obtained using multiwalled carbon-nanotube (CNT) cantilever switches. Continuum beam models like that developed here can be applied to CNT switches for nanotubes with more than ∼4–5 layers [4, 41]. In the experiments, typical CNTs had ∼25 layers with a 0.33 nm interlayer spacing. The height of the switch took values $\delta = 30$–800 nm and the beam length ranged from $l = 470$ to 1580 nm. Following the earlier comparison to experiments (section 3), we set the parameters in our numerical model to be $w^* = 0.33$ nm and $h = 8$ nm.

We reproduce the experimental data for a carbon beam–carbon substrate switch in figure 9 [17], together with the scaling law presented in the original paper, $\delta_{\text{clamp}} \sim l^4$ (dotted line). This scaling law was based on the assumption that stiction is determined by the total adhesive energy stored in the adhered segment of the beam, for a given point of delamination, λ [17]. However, as discussed above, λ is not known *a priori*. In fact, stiction boundaries should be found by solving for λ, which is dependent on the geometric and material parameters of the system. The resulting clamped and pinned stiction conditions (19) and (21) are shown in figure 9 (dashed and solid, respectively). Since the strength of carbon–carbon adhesion is not precisely known the figure shows a range of possible values for $\Delta\gamma$ in the range $0.01 \leq \Delta\gamma \leq 0.1$ J m^{-2}. We find generally good agreement between the experimental data and the stiction boundaries presented here.

5. Conclusions

We have presented a theoretical, quasi-static study of stiction processes in NEM contact switches. Incorporating the effects of geometrically nonlinear deflections and finite beam thickness, we discussed in detail the hysteresis loop that describes the closing/opening processes of a contact switch with changes in the applied voltage.

The hysteresis loop was found to consist of two kinds of processes: (a) the continuous evolution of a given state (freely suspended, pinned adhered or clamped adhered) and (b) discontinuous jumps between these three states at critical values of the applied voltage.

We found that pull-in (the transition from freely suspended to a contacting regime) can result in either a pinned or a clamped state. Suspended-to-pinned transitions are found to occur only for sufficiently thick sheets, and when the switch height lies within a given range. Outside this range, the beam will snap from the suspended state straight to a clamped configuration. We believe that the mode of transition may have important implications for the second main failure mechanism in NEM contact switches: ablation. In ablation the beam tip is damaged and the beam gradually shortens as the switch undergoes repeated ON/OFF cycles. Whether the initial contact with the bottom electrode occurs with a 'flat' or an angled tip is likely to affect this damage process. However, ablation failure is very much governed by the dynamic behaviour of the switch and hence is beyond the scope of this paper.

The pull-out behaviour of a system (the transition back to a free state) was shown to be governed by the critical heights $\delta_{\text{pin}}(l)$ and $\delta_{\text{clamp}}(l)$. If $\delta < \delta_{\text{clamp}}$, the switch will get stuck in the clamped state. For $\delta_{\text{clamp}} < \delta < \delta_{\text{pin}}$, the switch is expected to suffer non-volatile pinned stiction. If $\delta > \delta_{\text{pin}}$, on the other hand, the switch will return to its original open configuration, once the voltage is removed and the stiction is volatile, as desired.

By considering a linearized framework, analytical estimates of these critical heights were presented and compared to the results of our numerical model. We found close agreement between the two for a large range of switch aspect ratios. In particular, the commonly used analytical results present a practical and valid solution for values of δ/l up to ∼0.3. It also emerged that the stiction conditions are in good agreement with recent experimental data.

We further considered the critical pull-out voltages $\psi_{\text{pin}}^{(\text{min})}$ and $\psi_{\text{clamp}}^{(\text{min})}$. Since these minimum voltages were found to be consistently lower than the pull-in voltage, $\psi_{\text{p–i}}$, it is clear that significant hysteresis between free and adhered states exists. Also, the minimum clamped voltage, $\psi_{\text{clamp}}^{(\text{min})}$ was observed

to be always lower than the pinned-to-clamped transition voltage, $\psi_{\rm pin}^{(\max)}$, suggesting further hysteresis between the two adhered states. This lends further support to the idea that the dynamics of the respective transitions may play an important role with respect to the stability of the different states. We conclude that a study of the dynamic processes of the switch cycle would present an interesting starting point for future work.

Acknowledgments

This publication is based on work supported in part by Award No. KUK-C1-013-04, made by King Abdullah University of Science and Technology (KAUST). TJWW is supported by EPSRC and Cambridge Philosophical Society.

Appendix

In this appendix we derive the pinning condition (20). For a pinned state we have $\lambda = l$ and the boundary conditions are $w(l) = w''(l) = 0$, since the sheet is no longer flat at $x = l$ but instead experiences zero moment at the point of pinning. In this section we derive an analogue of the clamped delamination condition (18) appropriate for a pinned boundary condition. This is done by balancing the shear force acting on the beam at the point of pinning with the explicit van der Waals force acting near $x = l$.

We solve (17) subject to clamped conditions at $x = 0$ and pinned conditions at $x = l$, to find:

$$w(x) = \delta\left[1 + \frac{1}{2}\left(\frac{x}{l}\right)^2\left(\frac{x}{l} - 3\right)\right]. \tag{22}$$

For the angle and the shear force at the pinning point we have

$$\varphi \simeq w'(l) = -3\delta/2l, \qquad F_{\rm shear} = \mathcal{B}w'''(l) = 3\mathcal{B}\delta/l^3. \tag{23}$$

We aim to relate this shear force to the van der Waals force, $F_{\rm vdW}$ by utilizing the earlier result (5) which relates the macroscopic concept of adhesion to the short range vdW interaction. For pinned states, we expect these forces to cancel each other. Let us consider the van der Waals force per unit length, $f_{\rm vdW}$. From (6) and (5), we find that in the linear limit (and for $w^* \ll h$)

$$f_{\rm vdW} = -\tfrac{8}{3}\Delta\gamma a w^{*2}\left\{w_-^{-3} - w_+^{-3} - w^{*6}\left[w_-^{-9} - w_+^{-9}\right]\right\}, \tag{24}$$

where $w_- = w - h/2$ and $w_+ = w + h/2$. To get the total vdW force acting on the beam, $F_{\rm vdW}$, we integrate over the length of the beam. We assume that near contact (the only region where the van der Waals force is significant) the profile of the beam can be written as

$$w = w^* + h/2 + \varphi(l - x), \tag{25}$$

i.e. a straight line with contact distance of the mid-plane $w(l) = w^* + h/2$ and a slope φ. This is justified since there is no bending moment acting on the pinned end and all angles are taken to be small. Substituting (25) into (24) and integrating from $x = -\infty$ to l, we obtain an analytic, but cumbersome, expression for $F_{\rm vdW} = F_{\rm vdW}(\Delta\gamma, h, w^*)$. Since the vdW force is only significant very close to the pinning point the integral converges, even for small values of φ.

Performing a series expansion in w^*, we find

$$F_{\rm vdW} = \frac{\Delta\gamma}{\varphi}a\left[1 - \frac{4}{3}\left(\frac{w^*}{h}\right)^2 + \frac{8}{3}\left(\frac{w^*}{h}\right)^3 - \cdots\right]. \tag{26}$$

But since $w^* \ll h$, this gives to a good approximation $F_{\rm vdW} \simeq \Delta\gamma a/\varphi$.

We postulate that the boundary of non-volatile pinning is found at equilibrium between the shear force due to bending, $F_{\rm shear}$ and the short range vdW force acting at the pinned end, $F_{\rm vdW}$. Thus combining (23) and (26) and rearranging suitably gives following pinning condition:

$$|w'''(l)w'(l)| = 1/\ell_{\rm ec}^2. \tag{27}$$

Substituting this into (22) yields an expression for the critical pinning height (21):

$$\delta_{\rm pin} = (\sqrt{2}/3)l^2/\ell_{\rm ec}.$$

References

[1] Loh O and Espinosa H 2012 *Nature Nanotechnol.* **7** 283
[2] Osterberg P and Senturia S 1997 *J. Microelectromech. Syst.* **6** 107
[3] Chan E, Garikipati K and Dutton R 1999 *J. Microelectromech. Syst.* **8** 208
[4] Dequesnes M, Rotkin S and Aluru N 2002 *Nanotechnology* **13** 120
[5] Palasantzas G 2006 *J. Appl. Phys.* **100** 054503
[6] Rotkin S 2009 *Proc. SPIE* **7318** 731806
[7] Kinaret J, Nord T and Viefers S 2003 *Appl. Phys. Lett.* **82** 1287
[8] Dadgour H, Cassell A and Banerjee K 2008 *Electron Devices Meeting, 2008* (Piscataway, NJ: IEEE) pp 1–4
[9] Chakraborty S, Bhattacharya A and Bhattacharyya T 2011 *Micro Nano Lett.* **6** 43
[10] Mastrangelo C and Hsu C 1992 *Hilton Head* (Piscataway, NJ: IEEE) pp 208–12
[11] Mastrangelo C and Hsu C 1993 *J. Microelectromech. Syst.* **2** 33
[12] Mastrangelo C 1997 *Tribol. Lett.* **3** 223
[13] de Boer M and Michalske T 1999 *J. Appl. Phys.* **86** 817
[14] de Boer M, Knapp J, Michalske T, Srinivasan U and Maboudian R 2000 *Acta Mater.* **48** 4531
[15] van Spengen W, Puers R and De Wolf I 2002 *J. Micromech. Microeng.* **12** 702
[16] van Spengen W, Puers R and De Wolf I 2003 *IEEE Trans. Device Mater. Reliab.* **3** 167
[17] Loh O, Wei X, Ke C, Sullivan J and Espinosa H 2011 *Small* **7** 79
[18] Evans A A and Lauga E 2009 *Phys. Rev.* E **79** 066116
[19] Ramezani A, Alasty A and Akbari J 2007 *Nanotechnology* **19** 015501
[20] Oyharcabal X and Frisch T 2005 *Phys. Rev.* E **71** 036611
[21] Glassmaker N J and Hui C Y 2004 *J. Appl. Phys.* **96** 3429
[22] Wagner T J W and Vella D 2013 *Soft Matter* **9** 1025
[23] Bico J, Roman B, Moulin L and Boudaoud A 2004 *Nature* **432** 690
[24] Roman B and Bico J 2010 *J. Phys.: Condens. Matter* **22** 493101
[25] Landau L D and Lifschitz E M 1970 *The Theory of Elasticity* (Oxford: Pergamon)

[26] Audoly B and Pomeau Y 2010 *Elasticity and Geometry* (Oxford: Oxford University Press)
[27] Timoshenko S and Goodier J 1970 *Theory of Elasticity* (New York: McGraw-Hill)
[28] DelRio F W, de Boer M P, Knapp J A, Reedy E D, Clews P J and Dunn M L 2005 *Nature Mater.* **4** 629
[29] Yin Z and Ya-pu Z 2004 *Acta Mech. Solida Sin.* **17** 104
[30] Israelachvili J N 1992 *Intermolecular and Surface Forces* (London: Academic)
[31] Wagner T J W and Vella D 2012 *Appl. Phys. Lett.* **100** 233111
[32] Chowdhury S, Ahmadi M and Miller W 2005 *J. Micromech. Microeng.* **15** 756
[33] Gorthi S, Mohanty A and Chatterjee A 2006 *J. Micromech. Microeng.* **16** 1800
[34] Shin Y J, Stromberg R, Nay R, Huang H, Wee A T, Yang H and Bhatia C S 2011 *Carbon* **49** 4070
[35] Vella D, Boudaoud A and Adda-Bedia M 2009 *Phys. Rev. Lett.* **103** 174301
[36] Wang S, Zhang Y, Abidi N and Cabrales L 2009 *Langmuir* **25** 11078
[37] Zong Z, Chen C, Dokmeci M and Wan K 2010 *J. App. Phys.* **107** 026104
[38] Koenig S P, Boddeti N G, Dunn M L and Bunch J S 2011 *Nature Nanotechnol.* **6** 543
[39] Scharfenberg S, Mansukhani N, Chialvo C, Weaver R L and Mason N 2012 *Appl. Phys. Lett.* **100** 021910
[40] Majidi C 2007 *Mech. Res. Commun.* **34** 85
[41] Ru C 2000 *Phys. Rev.* B **62** 9973